Supporting Information:

On Localized Vapor Pressure Gradients Governing Condensation and Frost Phenomena

Saurabh Nath and Jonathan B. Boreyko

Department of Biomedical Engineering and Mechanics, Virginia Tech, Blacksburg, Virginia 24061, USA

Contents

1 Nomenclature **S2**

2 Relevant Equations **S4**

3 Comparison with Previous Studies: $SSD-\theta$ Plot **S6**

4 Comparison with Previous Studies: $\Delta T-\theta$ Plot **S7**

5 Subcooling Degree for Heterogeneous Nucleation **S8**

6 Supersaturation Pressure for Heterogeneous Nucleation **S9**

7 Thermodynamically Favored Mode of Heterogeneous Nucleation **S10**

8 Nucleation Pressure on Ice **S11**

1 Nomenclature

a	Height of the monolayer-thick disk shaped embryo nucleating on ice [m]
A_{ij}	Contact area of phase i with phase j [m^3]
$A_{\parallel}$	In-plane projected area of the daughter drop [m^2]; the area vector is parallel to the substrate
$A_{\perp}$	Out-of-plane projected area of the daughter drop [m^2]; the area vector is perpendicular to the substrate
d	Twice the radius of curvature of the liquid droplet being harvested by its neighboring ice droplet
D	Diffusivity of water vapor in air [m^2/s]
g	Acceleration due to gravity [m/s^2]
h_{ij}	Specific enthalpy for phase change [J/mol]
I	Embryo formation rate [$m^{-2}s^{-1}$]
I_c	Critical embryo formation rate [$m^{-2}s^{-1}$]
I_0	Kinetic constant of nucleation [$m^{-2}s^{-1}$]
$J_{l,c}$	Mass flux condensing on the daughter drop [kg/m^2-s]
$J_{l,e}$	Mass flux evaporating from the daughter drop [kg/m^2-s]
H	Relative humidity in the ambient
k	Boltzmann constant [J/K]
k_w	Thermal conductivity of water [W/m-K]
k_{silane}	Thermal conductivity of silane monolayer [W/m-K]
$k_{silicon}$	Thermal conductivity of silicon wafer[W/m-K]
L	Length of ice bridge [m]
L_{exp}	Experimentally measured ice bridge length [m]
L_{max}	Maximum possible length of an inter-droplet ice bridge [m]
L_s	Length scale of condensing surface [m]
m	Cosine of contact angle
m_{bridge}	Mass of inter-droplet ice bridge [kg]
m_l	Mass of the liquid drop which is being harvested by its neighboring ice droplet [kg]
$\dot{m}_{i,c}$	Mass flow rate of vapor condensing on the ice drop [kg/m^2-s]
$\dot{m}_{l,c}$	Mass flow rate of vapor condensing on the daughter drop [kg/m^2-s]
$\dot{m}_{l,e}$	Mass flow rate of vapor emanating from the daughter drop [kg/m^2-s]
n	Number of mother droplets which are nearest neighbors to a daughter drop on a condensing surface
N_a	Avogadro's number
$p_{a,d}$	Actual supersaturated vapor pressure around a liquid droplet [Pa]
$p_{i,0}$	Saturation vapor pressure of ice at 0° C

organized in alphabetical order

Nomenclature

$p_{n,i}$	Supersaturated vapor pressure required for nucleation on ice [Pa]
$p_{n,w}$	Supersaturated vapor pressure required for heterogeneous nucleation on a substrate at temperature T_w [Pa]
p_s	Saturation vapor pressure [Pa]
$p_{s,d}$	Saturation vapor pressure of liquid water [Pa] corresponding to the droplet temperature T_d
p_{s_i}	Saturation vapor pressure of ice [Pa]
$p_{s_i,w}$	Saturation vapor pressure of ice at wall temperature [Pa]
p_{s_l}	Saturation vapor pressure of liquid water [Pa]
$p_{s_l,w}$	Saturation vapor pressure of liquid water at wall temperature [Pa]
p_t	Pressure at triple point [Pa]
p_∞	Ambient vapor pressure [Pa]
q	Amount of heat flux flowing through the entire condensing surface [W/m^2]
q_d	Amount of heat flux flowing through a droplet [W/m^2]
Q_d	Rate of heat transfer across the droplet [W]
r	Radius of curvature of droplet [m]
r_d	Width of the monolayer-thick disk shaped embryo nucleating on ice [m]
r_m	Radius of curvature of mother droplets, which are pre-existing droplets (micron-sized or larger) on a condensing surface [m]
r^*	Critical radius of curvature of an embryo where nucleation is stable [m]
R	Universal gas constant [J/mol-K]
$\bar{R}$	Gas constant of water vapor [J/kg-K]
S	Supersaturation ratio, $p_\infty/p_{s,w}$
SSD	Supersaturation degree required for nucleation, $(p_{n,w} - p_{s,w})/p_{s,w}$
t_{silane}	Thickness of silane monolayer [m]
$t_{silicon}$	Thickness of silicon wafer[m]
T	Absolute temperature [K]
T_d	Temperature inside the droplet near vapor-droplet interface [K]
T_{DP}	Dew point temperature [°C]
T_i	Temperature at the vapor-ice interface [K]
T_t	Temperature at triple point [K]
T_w	Wall temperature [K]
T_∞	Ambient temperature [K]
v	Molar volume of water [m^3/mol]
v_b	Velocity of the ice bridge [m/s]
v_v	Velocity of vapor condensing onto the surface [m/s]
V	Volume of embryo [m^3]

The units given here are the ones used in calculations, not necessarily the ones shown in plots where they have been changed for better visualization.

Nomenclature

α	Volumetric thermal expansion coeffecient [K^{-1}]
β	Ratio of $A_{\parallel}$ to $A_{\perp}$
δ	Distance between a daughter drop and a mother drop on a condensing and/or subfreezing surface [m]
δ_{Cr}	Dry zone length, that is, critical inter-droplet distance between a daughter drop and a mother drop that can remain dry on a condensing and/or subfreezing surface [m]
$\bar{\delta}$	Harmonic mean of the inter-droplet distances of the mother drop from the daughter drop in a multi-drop system on a condensing surface[m]
$\bar{\delta}_{Cr}$	Mean dry zone length [m]
$\bar{\delta}^*_{Cr}$	Nondimensionalized mean dry zone length [m]
$\bar{\delta}_{exp}$	Experimental value of mean dry zone length [m]
$\Delta\bar{g}$	Specific Gibbs energy change [J/m^3]
ΔG	Total Gibbs energy change [J]
ΔG^*	Critical Gibbs energy change required for nucleating an embryo [J]
ΔT_{cond}	Temperature drop across a droplet due to conduction resistance [K]
ΔT_{silane}	Temperature drop across silane monolayer [K]
$\Delta T_{silicon}$	Temperature drop across silicon wafer[K]
ζ	Concentration boundary layer thickness [m]
ζ_h	Hydrodynamic boundary layer thickness [m]
θ	Contact angle [radians]
ν	Kinematic viscosity of air [m^2/s]
ρ_l	Density of liquid water drop [kg/m^3]
ρ_i	Density of ice droplet [kg/m^3]
$\sigma_{ij}, \sigma_{jk}, \sigma_{ki}$	Surface energy per unit area of phase i with respect to phase j, phase j with respect to phase k and phase k with respect to phase i respectively [J/m^2]
τ	Total time taken for an ice bridge to grow and connect to a neighboring drop [s]
τ_{exp}	Experimentally measured time of bridge growth [s]

2 Relevant Equations

The equations used for estimation of accurate saturation vapor pressure P (in Pa) of water and ice and latent heat of condensation h_{liq} (in J/mol) and desublimation h_{ice} (in J/mol)as a function of temperature T ((in J/mol)) with the appropriate correction terms are [1]:

For $236 < T < 273.16$ K

$$h_{liq} \approx 56579 - 42.212T + \exp\left\{0.119(281.6 - T)\right\} \tag{S1}$$

For $123 < T < 332$ K

$$\begin{aligned}\ln\left(p_{liq}\right) \approx\ & 54.842763 - 6763.22/T - 4.210\ln\left(T\right) + 0.000367T + \tanh\left\{0.0415(T - 218.8)\right\} \\ & + \left(53.878 - 1331.22/T - 9.44523\ln\left(T\right) + 0.014025T\right)\end{aligned} \tag{S2}$$

For $T > 30$ K

$$h_{ice} = 46782.5 + 35.8925T - 0.07414T^2 + 541.5\left\{ \exp(-T/(281.6 - T))\right\}^2 \tag{S3}$$

For $T > 110$ K

$$p_{ice} = \exp\left(9.550426 - 5723.265/T + 3.53068 \ln\left(T\right) - 0.00728332T\right) \tag{S4}$$

The equations used for surface energy (J/m^2) as a function of temperature are [2, 3]

$$\sigma_{l,v} = (75.7 - 0.1775(T - 273.15)) \times 10^{-3} \tag{S5}$$

$$\sigma_{i,v} = (99.5 - 0.075(T - 273.15)) \times 10^{-3}, \tag{S6}$$

where $\sigma_{l,v}$ is the surface tension of liquid water with respect to vapor and $\sigma_{i,v}$ is the surface tension of ice with respect to vapor and temperature T is in K.

3 Comparison with Previous Studies: $SSD-\theta$ Plot

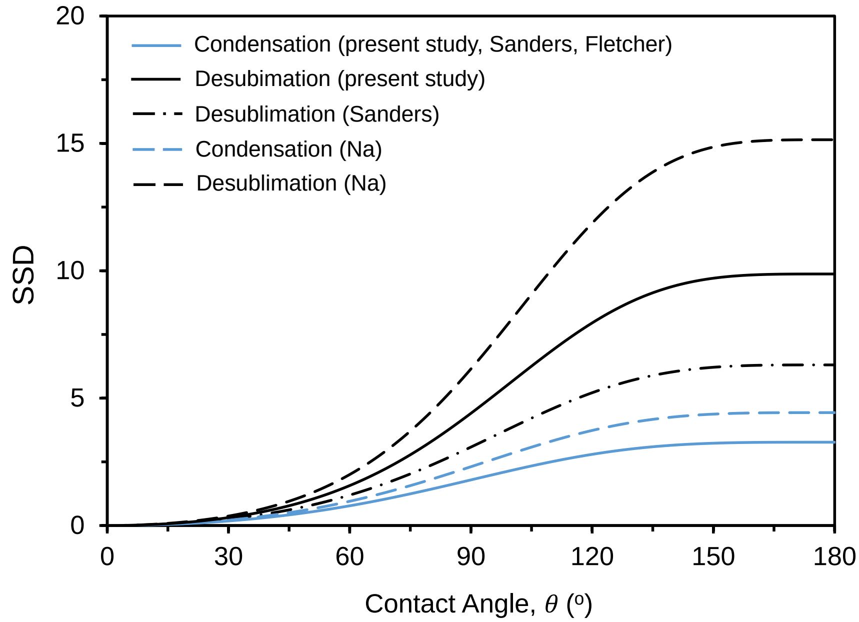

Figure S1: Comparison between the plots for supersaturation degree SSD as obtained by Sanders [2], Fletcher [4], Na [3] and present study. Note that the nature of all the curves in the same. In particular, our condensation curve is in perfect agreement with that of both Sanders and Fletcher. However the desublimation curve of Sanders is lower than that of ours and that of Na is higher. It is not entirely clear why the desublimation curves in particular have had such variation in the past, but a possible explanation could be the lack of accurate data on saturation vapor pressures on ice.

4 Comparison with Previous Studies: $\Delta T - \theta$ Plot

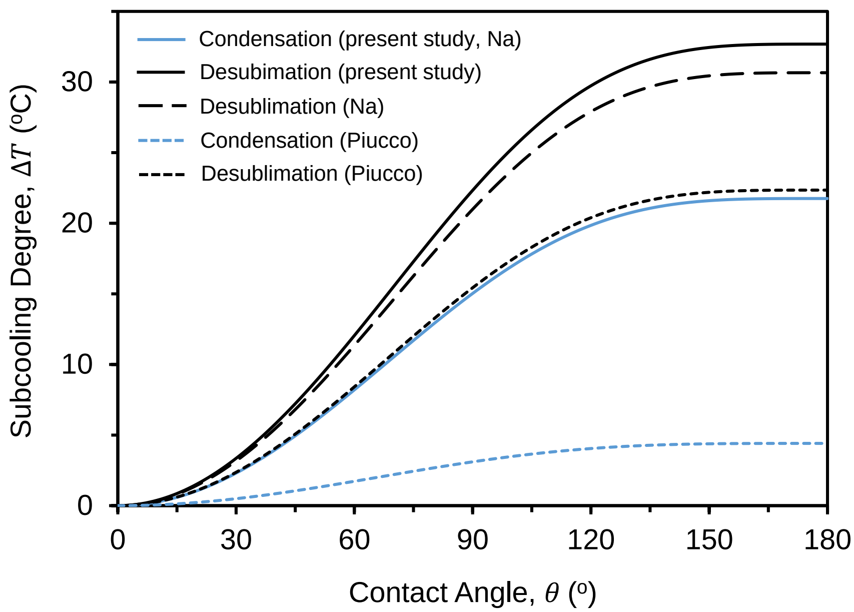

Figure S2: Comparison between the plots for subcooling degree as obtained by Piucco et al. [5], Na et al. [3] and present study. Note that our condensation curve is in perfect agreement with that of Na, however the desublimation curve of Na is slightly lower than that of ours. It appears likely that the significant under-prediction of Piucco et al. has stemmed from an error induced in their surface energy equations (Equations S5 and S6) where they have used T instead of $T - 273.15$ where T is the temperature in Kelvin.

5 Subcooling Degree for Heterogeneous Nucleation

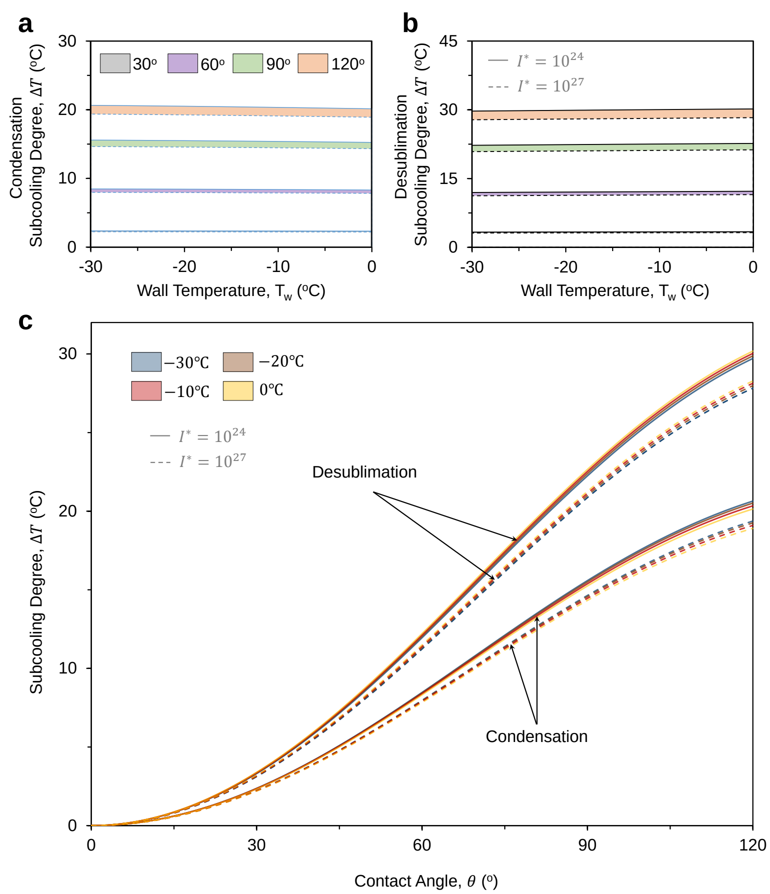

Figure S 3: Subcooling degree ΔT for condensation (a) and desublimation (b) as a function of wall temperature T_w for four different contact angles $\theta = 30°, 60°, 90°$C and $120°$C and two different embryo formation rates $I^* = 10^{24}$ and 10^{27}. (c) ΔT for both modes of nucleation as a function of wettability for wall temperatures $T_w = 0°$C,$-10°$C , $-20°$C and $-30°$C and embryo formation rates $I^* = 10^{24}$ and 10^{27}. Note that though both SSD and ΔT are analogous descriptions of heterogeneous nucleation, unlike SSD, ΔT remains fairly constant with temperature, for a given contact angle and mode of nucleation. This is why the $\Delta T - \theta$ curves for a given mode of nucleation and embryo formation rate almost collapse on each other. The weak dependence of ΔT with respect to T_w can be seen in the direction of change in color. This shows that though the subcooling degree for desublimation is higher than that for condensation, the extent of subcooling required is strongly dependent on the wettability of a substrate. All plots are solutions to Eq. 4, 8 and 9.

6 Supersaturation Pressure for Heterogeneous Nucleation

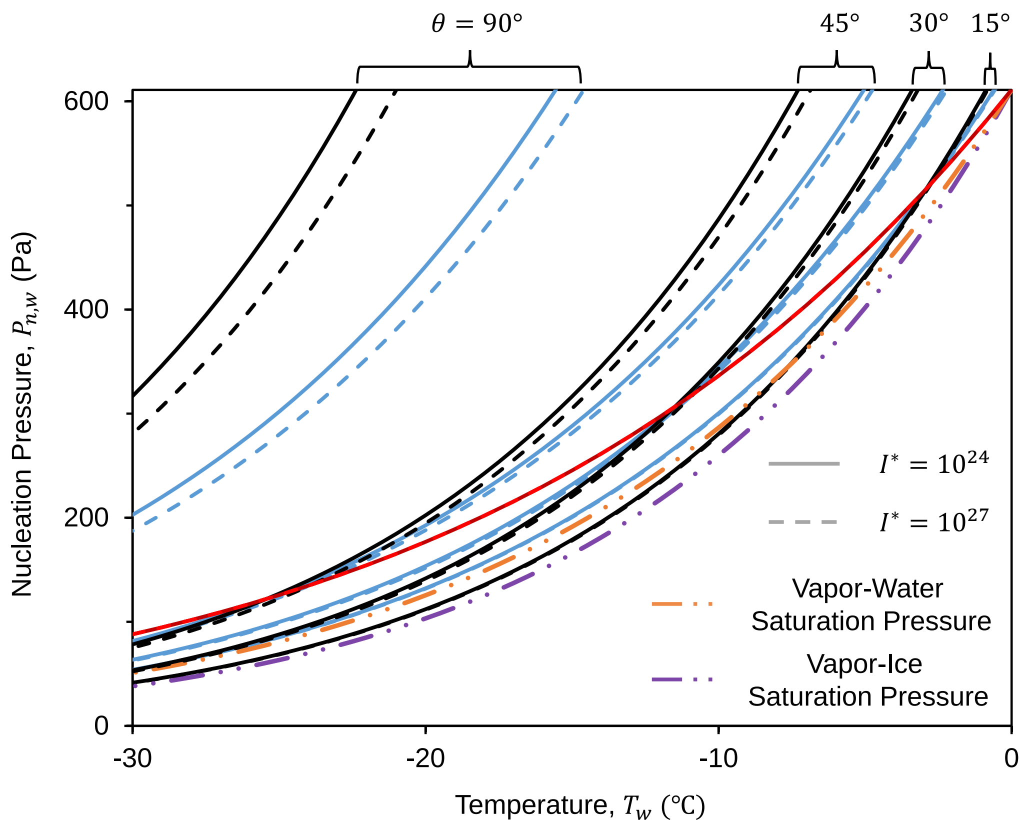

Figure S 4: Nucleation pressure $p_{n,w}$ required for condensation (blue lines) and desublimation (black lines) as a function of T_w for contact angles $\theta = 15°$, $30°$, $45°$, and $90°$ and embryo formation rates $I^* = 10^{24}$ and 10^{27}. The red dotted line is the locus of the intersection points of $p_{n,w}$ for the desublimation and condensation curves for contact angles ranging continuously from 0° to 120°, where desublimation is favored to the left (or below) and condensation to the right (or above) of the red line. As expected we see nucleation pressure decreases with T_w. Also note, the more hydrophyllic the substrate, the lesser is the pressure required for nucleation at a given T_w. It is also interesting to note that at extremely hydrophilic angles, for example, $\theta = 15°$, the desublimation nucleation pressure requirement dips below even the saturation vapor pressure of water for temperatures below $T_w \approx 10\,°\mathrm{C}$ (though always staying above the saturation vapor pressure above ice, as expected). This is strong evidence that indeed at low contact angles and sufficiently cold temperatures. In general, desublimation is the preferred mode of nucleation in the entire regime below the red line in where desublimation has a lower $p_{n,w}$ than that of condensation.

7 Thermodynamically Favored Mode of Heterogeneous Nucleation

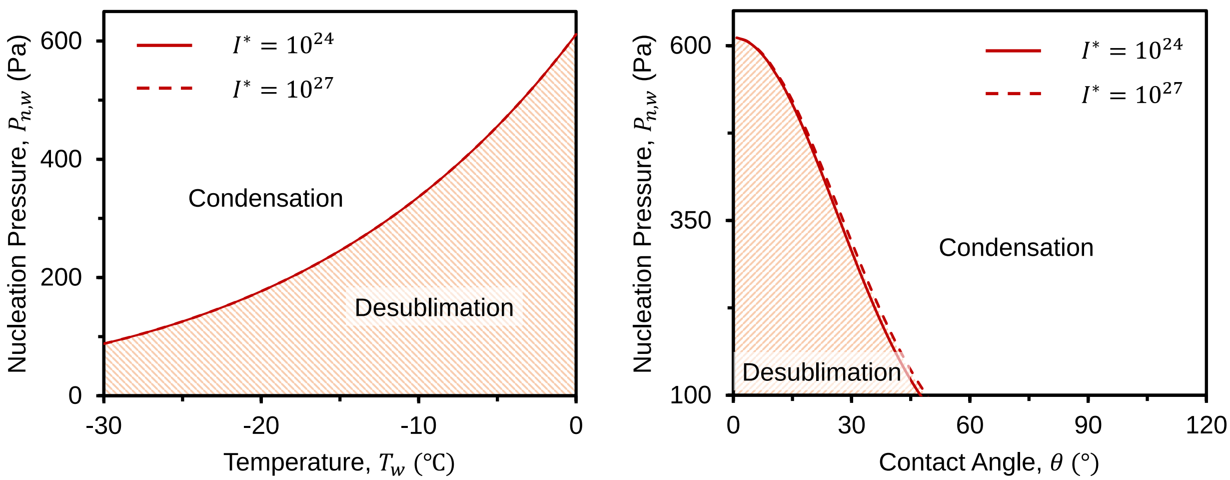

Figure S 5: (a) Phase diagram for the thermodynamically favored mode of nucleation for any pressure and surface temperature. Supercooled condensation is favorable in the phase space above the critical line and desublimation is preferred below. (b) Phase diagram for the same for any pressure and wettability, condensation being favored in the phase space to the right of the critical line and desublimation to the left. The solid lines correspond to $I^* = 10^{24}$ and the dashed lines correspond to $I^* = 10^{27}$. Note that these plots assume $\theta_{ice} = \theta_{water}$. In reality since on any substrate $\theta_{ice} > \theta_{water}$ [2], the red-lines will be shifted a bit lower than what we see in these plots.

8 Nucleation Pressure on Ice

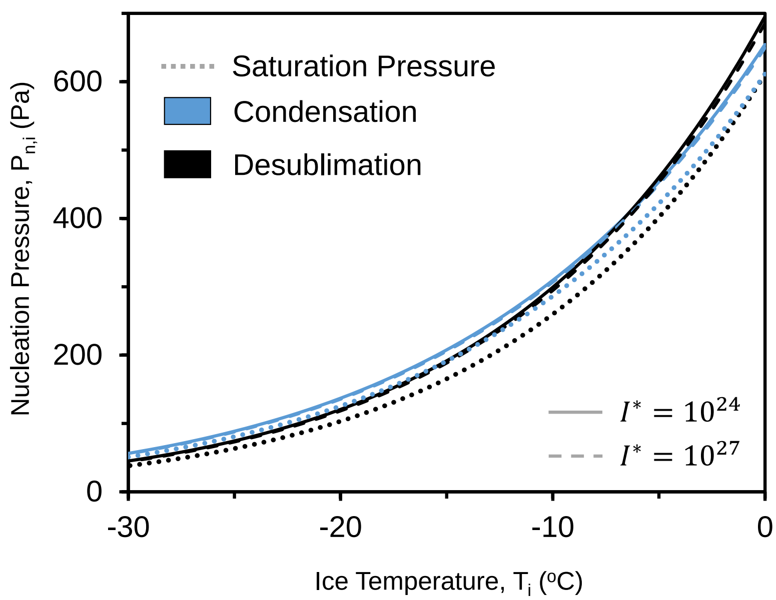

Figure S6: Vapor pressure required for nucleation $p_{n,i}$ on pre-existing ice as a function of the ice temperature. Blue/black lines represent the pressure to nucleate water/ice on ice when $I^* = 10^{24}$ (solid line), $I^* = 10^{27}$ (dashed line), or under saturated conditions (dotted lines). Assuming super-saturated conditions, condensation becomes the favorable mode of nucleation on ice above a critical temperature ($T_i > -6\,°\mathrm{C}$ for $I^* = 10^{24}$ or $I^* = 10^{27}$), while desublimation always exhibits a lower $p_{n,i}$ for nucleation occurring under approximately saturated conditions. However, embryo formation rates $I^* = 10^{24} - 10^{27}-$ are not applicable to the cases of nucleation on ice, as we show in our Results and Discussion Section.

References

[1] Murphy, D. M.; Koop, T. Review of the Vapour Pressures of Ice and Supercooled Water for Atmospheric Applications. *Q. J. R. Meteorol. Soc.* **2005**, *131*, 1539–1565

[2] Sanders, C. T. The Influence of Frost Formation and Defrosting on the Performance of Air Coolers. Ph.D. thesis, Delft University of Technology, 1974.

[3] Na, B.; Webb, R. L. A Fundamental Understanding of Factors Affecting Frost Nucleation. *Int. J. Heat Mass Transfer* **2003**, *46*, 3797–3808

[4] Fletcher, N. H. *Physics of Rain Clouds*; Cambridge University Press, Cambridge, UK, 1962

[5] Piucco, R. O.; Hermes, C. J. L.; Melo, C.; Barbosa, J. R. A Study of Frost Nucleation on Flat Surfaces. *Exp. Therm. Fluid Sci.* **2008**, *32*, 1710–1715